Journal of Power Sources 196 (2011) 9500–9509

Contents lists available at ScienceDirect

Journal of Power Sources

journal homepage: www.elsevier.com/locate/jpowsour

Analysis and optimization of solid oxide fuel cell-based auxiliary power units using a generic zero-dimensional fuel cell model

S. Göll*, R.C. Samsun, R. Peters

Forschungszentrum Jülich GmbH, Institute of Energy and Climate Research (IEK-3), D-52425 Jülich, Germany

ARTICLE INFO

Article history:
Received 15 February 2011
Received in revised form 29 April 2011
Accepted 10 July 2011
Available online 19 July 2011

Keywords:
APU
SOFC
Autothermal reformer
Process simulation
Design of experiments

ABSTRACT

Fuel-cell-based auxiliary power units can help to reduce fuel consumption and emissions in transportation. For this application, the combination of solid oxide fuel cells (SOFCs) with upstream fuel processing by autothermal reforming (ATR) is seen as a highly favorable configuration. Notwithstanding the necessity to improve each single component, an optimized architecture of the fuel cell system as a whole must be achieved. To enable model-based analyses, a system-level approach is proposed in which the fuel cell system is modeled as a multi-stage thermo-chemical process using the "flowsheeting" environment PRO/II™. Therein, the SOFC stack and the ATR are characterized entirely by corresponding thermodynamic processes together with global performance parameters. The developed model is then used to achieve an optimal system layout by comparing different system architectures. A system with anode and cathode off-gas recycling was identified to have the highest electric system efficiency. Taking this system as a basis, the potential for further performance enhancement was evaluated by varying four parameters characterizing different system components. Using methods from the design and analysis of experiments, the effects of these parameters and of their interactions were quantified, leading to an overall optimized system with encouraging performance data.

1. Introduction

The expansion of onboard convenience services such as entertainment, navigation or air conditioning and the substitution of mechanical or hydraulic components with electric units give rise to an increasing demand for supplementary electric power in road vehicles, ships and aircraft. Moreover, airplanes and long-haul trucks that require electricity during parking periods face public and legal pressure to reduce local emissions. Therefore, auxiliary power units (APUs) are gaining importance in the transportation sector. APUs efficiently supply electric power in the idle state and they avoid performance losses in the main engine of propulsion during normal operation. Particularly when they are based on fuel cell (FC) technology, auxiliary power units increase operation efficiency, generate near-zero emissions and are operated with low noise [1–4].

In contrast to batteries, FC-APUs are not constrained by limited operation ranges, provided that the fuel cell is operated with fuel that is available onboard. This implies on-site fuel processing for which typically one of the three main routes is applied: partial oxidation, steam reforming or autothermal reforming. The partial oxidation process (POX) is advantageous since no water is needed for the reforming process. However, partial oxidation of diesel or jet fuel often leads to carbon deposition. On the one hand, Lawrence and Boltze [5] successfully conducted start-up, load-change and shut-down tests with a sub-kW diesel fueled SOFC system including a POX reformer. On the other hand, stable operation could only be maintained for a few hours. Lindermeir et al. [6] tested an SOFC-APU containing a two-stage POX reformer exhibiting 260 W net electric power. However, using an alkane blend as fuel, no more than 9 h of successful operation could be demonstrated.

The main advantage of steam reforming is its high efficiency due to a higher hydrogen yield compared to POX. However, during the steam reforming of desulfurized diesel, Mengel et al. noticed a degradation of the catalyst due to soot depositions on the reactor components and heavy deposits on the catalyst's inner surface even within run times as short as 4 h [7]. Ming et al. [8] presented a steam reformer for ultra-low sulfur diesel (ULSD) operated at low temperatures ranging from 490 °C to 600 °C. Reportedly, conversion rates that partly exceeded 100% related to the C_1 products were obtained for 310 h on stream. More accurate values below 100%, achievable by additionally determining the residues, have not been reported. O'Connell et al. [9] implemented an oxidative steam reforming process to increase long-term stability and to reduce carbon depositions. This approach is similar to autothermal reforming,

* Corresponding author. Tel.: +49 2461 61 4394; fax: +49 2461 61 6695.
E-mail addresses: s.goell@fz-juelich.de (S. Göll), r.c.samsun@fz-juelich.de (R.C. Samsun), ra.peters@fz-juelich.de (R. Peters).

0378-7753/$ – see front matter © 2011 Elsevier B.V. All rights reserved.
doi:10.1016/j.jpowsour.2011.07.030

Nomenclature

c	element of design matrix, factor level indicator
e	relative effect
E	effect (variable units)
E_H^0	theoretical electric potential based on lower heating value (V)
F	Faraday constant (9.6485×10^4 A s mol^{-1})
Δg_R^0	change in Gibbs free energy due to reaction at standard pressure (J kg^{-1})
Δh_R	reaction enthalpy
K_{WGS}	equilibrium constant of water-gas shift reaction
LHV	lower heating value (J kg^{-1})
N	total number (of simulation runs)
$\dot{N}$	molar flow (mol s^{-1})
N_C	number of carbon atoms per molecule
P_e	electric power (W)
R	universal gas constant (8.314 J mol^{-1} K^{-1})
T	temperature (K)
U	voltage (V)
u_f	fuel utilization factor
y	molar fraction
Y	response variable (variable units)

Greek symbols

η_H^0	first-law efficiency (based on LHV)
η_{loss}	lumped cell voltage loss (V)
λ	normalized air-to-fuel ratio (lambda)
ν	stoichiometric coefficient

Subscripts

b	(after) burner
c	cathode
i	species i; factor i
in	inflow
j	counting variable for simulation runs
k	index of response variable
m	modified
N	Nernst-
s	stack
sys	system
out	outflow

however at a much lower air-to-fuel ratio (AFR). Based on a microchannel technology, they obtained over 98% conversion for diesel during 38 h of operation.

Autothermal reforming (ATR) can be considered as a compromise between partial oxidation and steam reforming. Kang et al. [10,11] experimentally investigated solid oxide fuel cell systems with diesel autothermal reforming reactors. However, fueling the laboratory-sized systems with a binary hydrocarbon mixture and with sulfur-free synthetic diesel, respectively, resulted in rapid and severe degradation due to incomplete conversion. Yoon et al. [12] published the results of experiments on the autothermal reforming of synthetic diesel fuel. They operated their reformer for approximately 1000 h with an LHV efficiency of 60% and observed no significant degradation in the performance of the reactor over time. Roychoudhury et al. [13] tested their microlith ATR reformer with jet fuel (JP-8) containing low sulfur (~15 ppm S) for 1100 h on stream. An analysis of the reformate showed that propane and propylene products remained below 10 ppm, resulting in a conversion rate of > 99.98%. Long-term experiments on autothermal reforming with commercial premium diesel and low-sulfur jet fuel (Jet A-1, <10 ppmw S) were performed by Pasel et al. [14] and Porš et al. [15]. They showed a conversion of 99.7% after 1000 h of operation with diesel and 99% after 2000 h with Jet A-1. In order to ensure high measurement accuracy, fuel conversion was determined based on carbon residues (C_2H_4, C_2H_6, C_3H_7, C_3H_8, $C_{4+}H_x$) in the dry gas phase and on the organic carbon content of the condensate withdrawn from the cooled product gas. At 1100 h of operation with Jet A-1, the mass of total organic carbon (OC) in the condensate was analyzed and found to be 70 mg OC per liter, corresponding to a conversion of 99.986%.

Clearly, the best reforming performances to date have been achieved using autothermal reforming. In comparison to POX and SR, longer operation times and higher conversion rates were achieved for middle distillates. Therefore, in this work, autothermal reforming was selected as the preferred route of reforming. Furthermore, different fuel cell technologies are available, ranging from low-temperature polymer electrolyte fuel cells to high-temperature solid oxide fuel cells. In the present study, we investigate APU systems on the basis of solid oxide fuel cells (SOFCs). Despite long start-up times, SOFCs have several advantages: there is no need for external cooling cycles, complex water management is avoided, and SOFCs impose the least stringent requirements on the upstream fuel processing compared to other fuel cell technologies [16,17].

The use of numerical simulation in product development is becoming increasingly important, since prototyping is expensive, time-consuming and incapable of exploring a greater number of design points and operating conditions. Consequently, numerical modeling of fuel-cell-based APU systems for transportation is an active field of research. Petruzzi et al. [18] modeled and simulated an SOFC system for APU applications but excluded the fuel processing steps. Dobbs et al. [19] analyzed an SOFC-based APU with autothermal reformer, using the commercial software GCTool from Argonne National Laboratory. Lawrence and Boltze [5] numerically examined the preliminary design of an SOFC-based APU with Matlab/Simulink®. Matlab/Simulink® was likewise used by Sorrentino and Pianese [20] for the control-oriented design and analysis of a hybrid SOFC APU. Baek et al. [21] examined SOFC systems including an autothermal reformer based on a Matlab® model of the SOFC, which was combined with an Aspen HYSYS® representation of the system. Baratto et al. [2] built an SOFC-APU model in AspenPlus® as a basis for cost estimation. Most recently, Santarelli et al. [4] conducted flight mission simulations of SOFC APUs based on a zero-dimensional system model, assuming that natural gas was available as fuel.

Many additional numerical studies can also be found for SOFC systems based on natural gas or biogas. Schlitzberger et al. [22] and Farhad et al. [23] performed simulations of SOFC systems based on their own codes. Bove et al. [24] developed a highly parameterized black-box SOFC model, which may be included in standard process simulation software such as AspenPlus®. Palsson [25] integrated a two-dimensional finite-volume model of the stack into AspenPlus® to enable simulation of an integrated SOFC and gas turbine system. Zhang et al. [26] proposed an SOFC model based solely on existing AspenPlus® units, which nevertheless requires a separate calculation of the stack voltage [27]. Similar models were developed by Panopoulos et al. [28] and Doherty et al. [29] in order to simulate biomass-fueled SOFC systems. A study including off-design analysis was presented by Riensche et al. [30]. The authors aimed to optimize a 200 kW combined heat and power (CHP) plant using the process simulation software PRO/II™, in which a user-defined stack model was included.

Despite the variety of available models, all of these approaches attempt to reproduce the characteristic current–voltage curves of fuel cells. This is accomplished by postulating reaction kinetics or equivalent electric circuits, which inevitably bear highly parameterized correlations that depend on geometric data as well as

on operation characteristics. The latter have to be determined experimentally for each particular fuel cell stack. However, during preliminary system development, final stack configurations have yet to be determined and there is often no measured data available. Moreover, one may attempt to conduct a general system analysis independent of a particular stack but focused on the system components and their interdependencies. For these purposes, we developed a new SOFC system model, which is presented in the following. It comprises all major components of integrated fuel cell systems and allows for simple and generic specification of the SOFC stacks.

2. Calculation

2.1. Scope and modeling principle

The auxiliary power units under consideration consist of an SOFC stack, a reformer, an anode off-gas burner (afterburner), a number of heat exchangers for heat integration and additional balance-of-plant components. These various system components have to be incorporated into a single simulation framework that must be simple enough to limit computational effort without compromising comprehensiveness, especially with regard to system interactions. The model was built into commercial process simulation software, so that existing material databases and pre-defined thermodynamic property calculation procedures could be used. PRO/II™ from Invensys Simsci-Esscor [31] was used for this purpose. As far as possible, the APU model was implemented based on existing unit operation modules contained in the software. This enhances design flexibility and facilitates comparative studies including variations of the system's process layout.

2.2. Solid oxide fuel cell

In this work, the operation of fuel cells with reformate is assumed, so that hydrogen and carbon monoxide constitute the effective fuel gases. As shown by Achenbach and Riensche [32] and Andreassi et al. [33], CO is directly oxidized at SOFC anodes. Consequently, two net electrochemical reactions have to be considered:

$$2H_2 + O_2 \rightarrow 2H_2O \quad (1)$$

$$2CO + O_2 \rightarrow 2CO_2 \quad (2)$$

Furthermore, due to the catalytic activity of the Ni-containing anode, the following two equilibrium reactions proceed simultaneously [34].

Steam reforming of methane:

$$CH_4 + H_2O \rightarrow CO + 3H_2 \quad (3)$$

Water-gas shift reaction:

$$CO + H_2O \rightarrow CO_2 + H_2 \quad (4)$$

In the present model, the species mass balances and the energy balance of the complete fuel cell stack are solved as a function of reaction rates and reaction enthalpies based on the reactions (1)–(4). In other words, the SOFC is represented by a single control volume. However, the progression of the reactions strongly depends on the internal geometric structures as well as on the material properties. Thus, in order to sustain a zero-dimensional model, four additional assumptions and simplifications are introduced:

A1. Ideal isothermal operation of the entire fuel cell stack;
A2. Water-gas shift equilibrium is prevalent everywhere in the stack;
A3. Methane steam reforming proceeds to equilibrium;

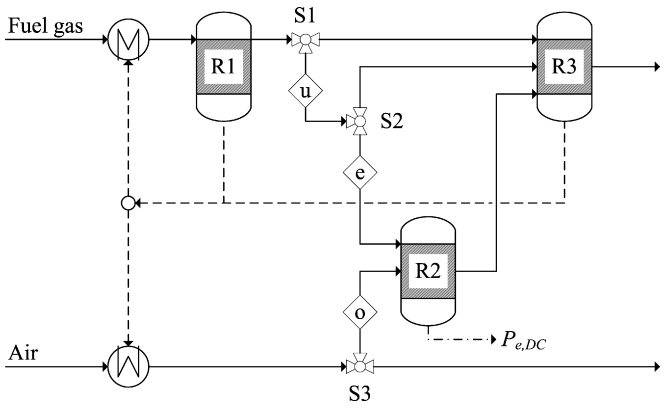

Fig. 1. Schematic flow sheet of the SOFC sub-model including Gibbs minimization reactors (R1, R2, R3), splitters (S1, S2, S3), controlled gas streams (u, e, o) and heat fluxes (dashed lines).

A4. Effective stack voltage and overall stack current adjust independent of each other.

Assumption A2 is generally in agreement with the literature (cf. [27,32]). Although assumption A3 is in contrast to the fact that methane steam reforming is kinetically controlled and subject to rate-limiting diffusion effects [32,35], it nevertheless provides a satisfactory approximation [36,37] and automatically considers the possible reverse reaction, i.e. methanation. As will be shown later, assumption A4 implies the specification of an effective stack voltage and the definition of a fixed fuel utilization factor.

For modeling purposes, the SOFC stack is conceived as a multistage process, the flow sheet of which is outlined in Fig. 1. First, reformate and air are brought to the specified operation temperature of the stack according to A1. Each of the three consecutive reaction stages is represented by an isothermal *Gibbs minimization reactor*, i.e. the equilibrium composition of the reaction products is calculated based on the principle of minimizing the Gibbs energy at constant temperature [38,39]. In the first reactor (denoted 'R1' in Fig. 1), the water-gas shift reaction and methane steam reforming simultaneously proceed to equilibrium. Subsequently, incomplete fuel utilization is accounted for by dividing the fuel gas into two branches in splitter 'S1'. The splitting factor is equal to the fuel utilization factor u_f defined as follows:

$$u_f = 1 - \frac{\dot{N}_{H_2,out} + \dot{N}_{CO,out}}{\dot{N}_{H_2} + \dot{N}_{CO}} \quad (5)$$

Once specified as a fixed input parameter to the model, u_f further determines the amount of oxygen that permeates through the solid electrolyte:

$$\dot{N}_{O_2,o} = \frac{1}{2} u_f (\dot{N}_{H_2} + \dot{N}_{CO}) \quad (6)$$

As can be seen in Fig. 1, the cross-electrolyte flow is represented by a stream of pure molecular oxygen ('o'), which is separated from the incoming air stream in *stream calculator* 'S3'.

In the fuel cells, the oxidation reactions release heat and electric power. The ratio of electric power to the total energy release can be described by a first-law efficiency, which depends on voltage and operation temperature (T_s):

$$\eta^0_{H,i}(T_S) = \frac{U}{E^0_{H,i}(T_s)}, \quad i = H_2, CO \quad (7)$$

The denominator in Eq. (7) contains the theoretical electric potentials of electrochemical oxidation of hydrogen or carbon monoxide,

respectively. These are calculated based on tabulated data of temperature-dependent heat of formation [40]:

$$E^0_{H,i}(T_S) = \frac{-\Delta h_{\mathrm{Ox},i}(T_S)}{2F}, \quad i = \mathrm{H_2}, \mathrm{CO} \tag{8}$$

In the present model, Eq. (7) is used to define a stream that only contains H_2 and CO. This stream, denoted 'e' in Fig. 1, is removed from the utilized fuel gas stream 'u' and is subsequently supplied to reactor 'R2' where complete oxidation takes place. Consequently, the resulting reaction enthalpy, i.e. the *heat duty* of 'R2', is equal to the electric power delivered by the stack:

$$\begin{aligned} P_e &= U \cdot 2\,\mathrm{F}u_f(\dot{N}_{\mathrm{H_2}} + \dot{N}_{\mathrm{CO}}) \\ &= -u_\mathrm{F}[(\eta^0_{H,\mathrm{H_2}}\dot{N}_{H_2})\Delta h_{R,\mathrm{H_2}} + (\eta^0_{H,\mathrm{CO}}\dot{N}_{\mathrm{CO}})\Delta h_{R,\mathrm{CO}}] \end{aligned} \tag{9}$$

The remaining fuel gas is fed to reactor 'R3', the calculated enthalpy difference of which thus corresponds to the heat released inside the stack. A reaction-independent minimization of the Gibbs energy is carried out [39], so that the product gas leaves 'R3' in overall chemical equilibrium, including the water-gas shift reaction.

As initially stated, all reaction stages are modeled as isothermal units. On the other hand, the stack as a whole is assumed to be ideally insulated. Applying the energy conservation principle to the stack consequently imposes a constraint on the only remaining independent variable, which is the flow rate of air to the cathode. The air flow rate, which is required to sustain the specified outlet temperature, is expressed in terms of lambda, i.e. the normalized air-to-fuel ratio:

$$\lambda_c = \frac{y_{\mathrm{O_2}}\dot{N}_{\mathrm{air}}}{\dot{N}_{\mathrm{O_2,o}}} \geq 1 \tag{10}$$

So far, it was assumed that a constant voltage is sufficient to describe the fuel cell characteristics. However, if the fuel gas compositions change due to alterations of the process layout, this assumption is oversimplifying and will thus distort comparative analyses. Therefore, a voltage correction is introduced, which is based on the composition dependency of the Nernst voltage. Generally, the actual voltage U is related to the Nernst voltage U_N through

$$U = U_N - \eta_{\mathrm{loss}} = \frac{-\Delta g^0_R}{2F} + \frac{RT}{2F}\ln\left(\prod_i y_i^{\nu_i}\right) - \eta_{\mathrm{loss}} \tag{11a}$$

The definition of the Nernst voltage contained in Eq. (11a) is based on the assumption of ideal gases, isothermal and isobaric conditions. The change of the specific Gibbs energy is a reaction-dependent constant, while the logarithmic term accounts for the effect of the actual mixture composition, expressed in terms of the molar fractions y_i of the reacting gases and the stoichiometric coefficients ν_i of the corresponding reaction. The lumped voltage drop η_{loss}, which takes into account the ohmic losses and the cathodic and anodic overpotentials, does not have to be determined explicitly within the present modeling framework. Rather it is important to note that η_{loss} is assumed to be unaffected by composition changes. With regard to the electrochemical reactions relevant in the SOFC, i.e. oxidation of H_2 and CO, Eq. (11a) takes the following forms:

$$U = \frac{-\Delta g^0_{\mathrm{H_2}}}{2F} - \eta_{\mathrm{loss,H_2}} - \frac{RT}{2F}\ln\left(\frac{y_{\mathrm{H_2O}}}{y_{\mathrm{H_2}}y^{0.5}_{\mathrm{O_2}}}\right) \tag{11b}$$

$$U = \frac{-\Delta g^0_{\mathrm{CO}}}{2F} - \eta_{\mathrm{loss,CO}} - \frac{RT}{2F}\ln\left(\frac{y_{\mathrm{CO_2}}}{y_{\mathrm{CO}}y^{0.5}_{\mathrm{O_2}}}\right) \tag{11c}$$

Both reactions generate the same voltage, which is due to the equipotential character of the electrode surfaces. Thermodynamically, the voltage equality is assured by the composition-dependent terms in Eqs. (11b) and (11c), which are correlated by the water-gas shift equilibrium:

$$K_{\mathrm{WGS}} = \frac{y_{\mathrm{CO_2}}y_{\mathrm{H_2}}}{y_{\mathrm{CO}}y_{\mathrm{H_2O}}} \tag{12}$$

Eq. (12) contains the equilibrium constant K_{WGS}, which only depends on temperature and with which Eq. (11c) can be rewritten:

$$U = \frac{-\Delta g^0_{\mathrm{CO}}}{2F} - \eta_{\mathrm{loss,CO}} - \frac{RT}{2F}\ln(K_{\mathrm{WGS}}) - \frac{RT}{2F}\ln\left(\frac{y_{\mathrm{H_2O}}}{y_{\mathrm{H_2}}y^{0.5}_{\mathrm{O_2}}}\right) \tag{13}$$

Comparing Eqs. (11b) and (13) clearly shows that if the compositions of the anode or cathode feed gas are altered as a result of a modified process layout, the voltages resulting from both reactions are offset uniformly. The corrected voltage U_m can thus be determined as a function of the specified reference voltage U and the composition alterations of H_2, O_2 and H_2O:

$$U_m = U - \frac{RT}{2F}\ln\left(\frac{y_{m,\mathrm{H_2O}}}{y_{m,\mathrm{H_2}}y^{0.5}_{m,\mathrm{O_2}}}\frac{y_{\mathrm{H_2}}y^{0.5}_{\mathrm{O_2}}}{y_{\mathrm{H_2O}}}\right) \tag{14}$$

The voltage correction accounts for deviations from a reference state that is associated with the molar fractions y_i of the feed gases, and for which the reference voltage U is defined. If the feed gas composition is changed from y_i to $y_{m,i}$, the modified voltage U_m has to be considered instead of U. Strictly speaking, the molar fractions contained in Eq. (14) refer to local conditions. For the present zero-dimensional model, however, only inlet and outlet conditions are known. In this case, taking the arithmetic mean values provides a satisfactory approximation [24].

2.3. Reformer

It is assumed that fuel processing is accomplished by autothermal reforming (ATR) because, as stated in the introduction, it provides the best long-term stability when diesel or jet fuel is used. Autothermal reforming comprises both exothermic partial oxidation

$$\mathrm{C}_n\mathrm{H}_m + \frac{n}{2}\mathrm{O_2} \rightarrow n\,\mathrm{CO} + \frac{m}{2}\mathrm{H_2} \tag{15}$$

and endothermic steam reforming

$$\mathrm{C}_n\mathrm{H}_m + n\,\mathrm{H_2O} \rightarrow n\,\mathrm{CO} + \left(n + \frac{m}{2}\right)\mathrm{H_2} \tag{16}$$

Furthermore, side reactions have to be taken into account, most importantly the water-gas shift reaction (reaction (4)) and methanation [35,41]:

$$\mathrm{CO} + 3\mathrm{H_2} \rightarrow \mathrm{CH_4} + \mathrm{H_2O} \tag{17}$$

The ATR model refers to an apparatus described by Pasel et al. [14], albeit without an integrated steam generator. The flow sheet of the model is outlined in Fig. 2. In contrast to the physical apparatus, air and liquid fuel are mixed first before steam is added. This allows the internal heat transfer from the reaction zone to the two cold inlet streams (air and fuel) to be modeled using a single heat exchanger. The *heat duty* of this unit is controlled such that the temperature of the gaseous fuel-steam-air mixture is equal to measured data.

Since exothermic partial oxidation proceeds much faster than endothermic steam reforming, a non-uniform axial temperature distribution along the monolith is observed, affecting the equilibrium reactions (4) and (17) [14,42]. Therefore, the ATR sub-model comprises two reaction stages in order to account for the different temperature levels. Each reaction zone is modeled on the basis of a *Gibbs minimization reactor*. In the first reactor unit, denoted 'Z1' (Fig. 2), equilibrium of all reactions is calculated by minimizing

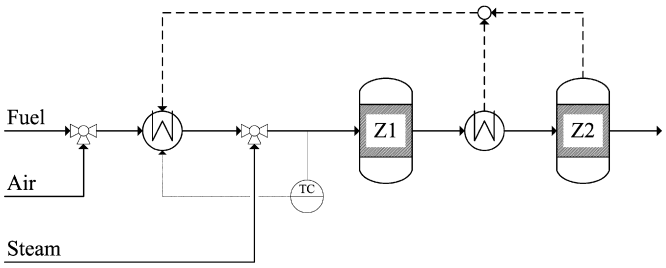

Fig. 2. Schematic flow sheet of the ATR sub-model including two reaction zones represented by Gibbs minimization reactors (Z1, Z2), internal heat fluxes (dashed lines) and control of heat balance (TC, dotted line).

the Gibbs energy and assuming adiabatic conditions. This leads to complete conversion of the liquid fuel due to partial oxidation and steam reforming. The second reactor ('Z2') is an isothermal unit, whose operating temperature corresponds to the outlet temperature of the autothermal reforming reactor. The temperature drop is accomplished in an intermediate heat exchanger, the outlet temperature of which is adjusted by means of a *controller*. The latter is specified such that the overall heat balance of the ATR, which is assumed to be ideally insulated, is satisfied.

2.4. Auxiliary system components

The SOFC stack and autothermal reformer are the two main components of the APU system. Nevertheless, additional system components are required to operate the fuel cell system. The following auxiliary components are included:

- afterburner,
- heat exchangers,
- condenser and separator,
- pumps, blowers and compressors.

An afterburner is needed to ensure low-to-zero-emission exhaust since the fuel gas is only incompletely utilized by the fuel cells. A single adiabatic *Gibbs minimization reactor* is used to model the burner. The calculated product temperature corresponds to a theoretical peak temperature, which in practice should be kept below 950 °C due to material constraints. This is accomplished by controlling the amount of cold excess air. The corresponding lambda value is defined as follows:

$$\lambda_b = \frac{y_{O_2}\dot{N}_{air}}{0.5(y_{H_2} + y_{CO} + 4y_{CH_4})\dot{N}_{anode\text{-}off}} \geq 1 \quad (18)$$

Heat exchangers are needed mainly for the purpose of heat integration. Moreover, heat exchanger units have been introduced in the sub-models of Figs. 1 and 2 in order to represent internal heat transfer. To all of these units an overall heat transfer coefficient of 100 $W\,m^{-2}\,K^{-1}$ is assigned. With the use of micro-structured heat exchangers, even higher overall heat transfer coefficients were achieved experimentally [43]. At 150 $W\,m^{-2}\,K^{-1}$, however, the pressure drop already exceeded 180 mbar. Therefore, the more conservative value of 100 $W\,m^{-2}\,K^{-1}$ was assumed in order to comply with an allowable pressure drop of 50 mbar (cf. Table 1), which was reached in [43] using a micro-structured heat exchanger. All heat exchangers are modeled using the PRO/II^{TM} unit *simple heat exchanger*. In order to be able to estimate the required minimum heat exchanging area, ideal countercurrent operation is presumed.

Autothermal reforming requires a constant supply of water. Therefore, the APU system must contain a closed water cycle in order to be self-sufficient, which is realized by installing a combined condenser and water separator. This water recovery unit is modeled on the basis of an isothermal *flash*, which calculates the vapor-liquid equilibrium at constant temperature based on the non-random two-liquid (NRTL) activity coefficient model [44]. The solubility of supercritical gases is considered by applying Henry's law. The temperature of the *flash*, which is needed to match the mass flow of condensed water with the water requirement of the ATR, is adjusted by a *controller*.

Table 1
Pressure losses assigned to individual system components.

System component	Pressure loss (mbar)	System component	Pressure loss (mbar)
SOFC stack		Afterburner	
Anode side	20	Combustion chamber	20
Cathode side	30	Heat exchanger	
ATR		Vaporization of water	500
Monolith	70	All other streams	50
Air supply	30	Condenser	
Liquid fuel atomizer	5000	Moist gas	50
		Air cooler	3

Finally, pumps, blowers and compressors are needed to overcome pressure losses in the system. Blowers and compressors are both modeled using the PRO/II^{TM} unit *compressor*, to which a constant isentropic efficiency is assigned. The compressor efficiencies assumed in the literature typically range from 60% to 75% [2,20,23,28]. In this work an isentropic efficiency of 60% is used for the base case. Since this is a rather conservative estimate, the effect of increased compressor efficiency on the overall system performance will furthermore be examined in section 4.2. The efficiency of liquid *pumps* is assumed to be 70%, a value characterizing well dimensioned equipment [45]. The back pressures that must be overcome are different at each stream inlet. In the present study, the corresponding values are determined by assigning specific pressure losses to all flow sheet units according to Table 1.

3. System layouts

The first part of our study comprises a comparative study of different system layouts. A base system is built as a reference point. This base system and four selected alternative designs are presented in this section. They will serve as a basis for the process analysis and optimization described in Section 4.

3.1. Base system

The flow sheet of the reference system is shown in Fig. 3. The autothermal reforming reactor is fed with air and liquid fuel at

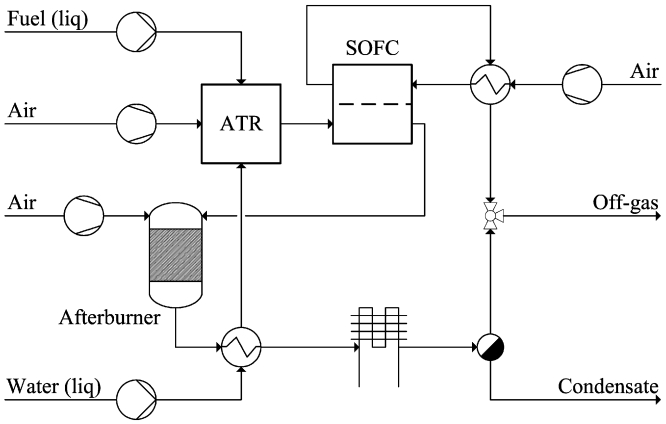

Fig. 3. Flow sheet of the reference system.

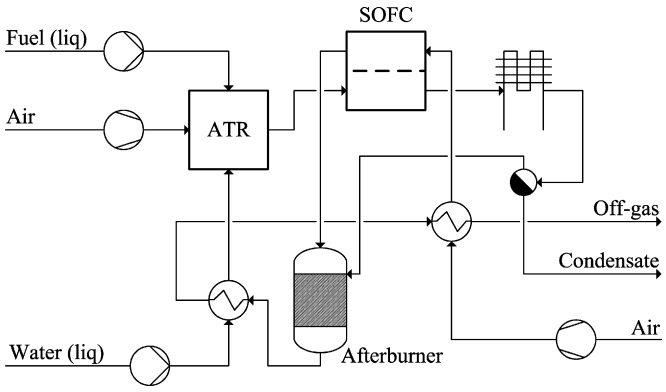

Fig. 4. Flow sheet of system alternative 1.

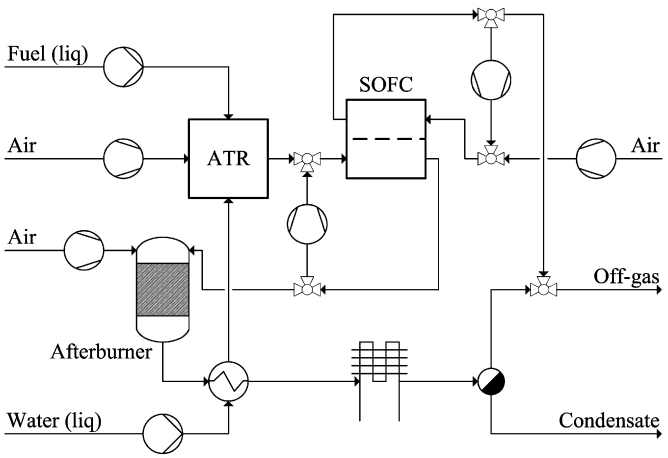

Fig. 5. Flow sheet of system alternative 4.

ambient temperature, while water enters the ATR in the form of superheated steam, which is generated using the hot burner exhaust gas. The product gas of the ATR (reformate) feeds the anode of the SOFC. The cathode is provided with moist air, which is pre-heated by hot cathode off-gas. Ambient air is assumed to contain 20% oxygen, 2% water vapor (molar basis) and nitrogen. The anode off-gas is directed to the afterburner, which is operated with additional ambient air. Fresh air is used in the afterburner for two reasons: First, the burner is positioned far downstream, so that a low-power blower can be applied economically. Second, cold air most efficiently limits the adiabatic combustion temperature inside the burner. After passing through the heat exchanger to generate superheated steam, the exhaust is cooled down in an air-cooled condenser.

3.2. System variations

3.2.1. Modified operation of the afterburner

The first variation comprises the operation of the afterburner with cathode off-gas instead of fresh air. Since considerable excess air is used for stack cooling, a large stream of cathode off-gas is available, which always contains enough oxygen. The large flow rate, however, results in a significant reduction in the partial pressure of the water vapor in the burner exhaust gas. Consequently, the condensation of water, which is necessary to close the water cycle, becomes challenging. Thus, the condenser is installed between the SOFC stack and the afterburner in order to take advantage of the higher water content in the anode off-gas. The resulting system layout of alternative 1 is depicted in Fig. 4.

3.2.2. Systems including recycles

Three more system variations are considered, all of which include recycle streams. Cathode off-gas recycling can generally be used to replace the cathode-air pre-heater [30,46]. In return, a hot-temperature blower has to be installed in order to overcome the pressure drop inside the recirculation loop. The recycle ratio is controlled such that the temperature at the cathode inlet does not fall below a threshold value, which is determined by the maximum allowable difference to the operation temperature of the stack: $\Delta T = 150\,\mathrm{K}$.

Recirculation of anode off-gas to the anode inlet is applied to reuse a portion of the initially unutilized fuel [21]. In the present study, the recirculation ratio of anode recycling is fixed to a value of 0.5 – a tradeoff between increased overall fuel utilization, on the one hand, and decreased stack voltage (Eq. (14)) as well as the increased power need of the hot-gas blower, on the other hand. In the presence of anode recycling, two different fuel utilization factors are distinguished: Stack utilization is defined by the inlet and outlet streams, which are directly attached to the SOFC stack. In contrast, system utilization is determined by a control volume that encompasses the stack as well as the recycle loop.

In this work, three configurations including recycles are examined:

- Single anode recycle (alternative 2).
- Single cathode recycle (alternative 3).
- Combined anode and cathode recycle (alternative 4).

The flow sheet of alternative 4 is shown in Fig. 5.

4. Results and discussion

4.1. Conceptual study

All four system variations and the base system were evaluated separately and then compared to each other. The key parameter for evaluating system performance was the net electric efficiency. It is defined based on the lower heating value (LHV) of the liquid fuel:

$$\eta_{\mathrm{sys}} = \frac{P_{e,\mathrm{AC,net}}}{\dot{m}_{\mathrm{fuel}} \cdot \mathrm{LHV}_{\mathrm{fuel}}} = \frac{\eta_{\mathrm{DC/AC}} \cdot P_{e,\mathrm{DC}} - P_{e,\mathrm{loss}}}{\dot{m}_{\mathrm{fuel}} \cdot \mathrm{LHV}_{\mathrm{fuel}}} \tag{19}$$

The parasitic power loss $P_{e,\mathrm{loss}}$ considers all electric consumers in the system, i.e. pumps and compressors. It was presumed that all system-intrinsic consumers run on alternating current. The efficiency of the DC/AC converter $\eta_{\mathrm{DC/AC}}$ was assumed to be equal to 95%.

For the evaluation and comparison of the different system layouts, equal operating parameters as well as operating conditions were used: The feed streams are available at ambient conditions, i.e. at 1.01 bar and 25 °C. The relative humidity of the surrounding air was assumed to be 60%. All systems were operated with a fixed fuel feed of 1.2 kg *n*-dodecane per hour. The air feed to the ATR is specified by the ratio of molecular oxygen to the number of carbon atoms contained in the fuel:

$$\frac{n(\mathrm{O_2})}{n(\mathrm{C})} = \frac{\dot{N}_{\mathrm{O_2}}}{\dot{N}_{\mathrm{fuel}} \cdot N_{\mathrm{C}}} \tag{20}$$

The required feed of water is defined by the steam-to-carbon ratio:

$$\frac{n(\mathrm{H_2O})}{n(\mathrm{C})} = \frac{\dot{N}_{\mathrm{H_2O}}}{\dot{N}_{\mathrm{fuel}} \cdot N_{\mathrm{C}}} \tag{21}$$

The values were set to $n(\mathrm{O_2})/n(\mathrm{C}) = 0.47$ and $n(\mathrm{H_2O})/n(\mathrm{C}) = 1.9$, respectively. Under these conditions, a long-term experiment [14] demonstrated the stability of the reforming activity with 99% conversion of desulfurized Jet A-1 fuel after 2000 h. The steam further

Table 2
Summary of simulation results of the conceptual study.

	Base case	Alt. 1	Alt. 2	Alt. 3	Alt. 4
System					
Net electric efficiency (%)	29.2	28.9	31.4	29.6	32.0
Net electric power (AC) (kW)	4.30	4.25	4.62	4.35	4.71
Parasitic losses (kW)	0.54	0.58	0.65	0.41	0.49
Fuel utilization (%)	75.0	75.0	85.7	75.0	85.7
SOFC					
Voltage (mV)	700	700	667	691	658
Gross elect. power (DC) (kW)	5.1	5.1	5.5	5.0	5.5
Lambda	8.7	8.7	9.4	2.1	2.2
Air standard flow rate ($m^3\ h^{-1}$)	66.3	66.5	82.2	15.8	19.6
Burner: air standard flow rate ($m^3\ h^{-1}$)	5.9	–	2.0	5.9	2.0
Overall off-gas					
Standard flow rate ($m^3\ h^{-1}$)	77.7	72.0	89.7	27.2	27.0
Temperature (°C)	171	201	182	417	506
Condensation temperature (°C)	57	59	64	57	64
Total heat exchanging area (m^2)	1.77	1.88	1.86	0.86	0.72

has to be supplied to the ATR at a specified temperature of 480 °C. The reference voltage of the SOFC stack according to the conditions in the base system was defined as $U = 0.7$ V. The fuel utilization factor of the stack was always equal to 0.75, and the uniform operating temperature was assumed to be 750 °C.

The main results of the comparative study are summarized in Table 2. Net electric efficiency, net electric power output of the system, parasitic losses due to system consumers and gross electric power of the SOFC stack correspond to Eq. (19). The effective stack voltage was calculated using Eq. (14). The required standard flow rate of cathode air and the normalized air-to-fuel ratio lambda are related to each other through Eq. (10). The effective off-gas comprises the exhaust gas from the afterburner and spent cathode air. The indicated condensation temperature is a threshold value for water autarky. Finally, the total heat exchanger area given in Table 2 comprises heat exchangers for steam generation, condensation and, except for process alternatives 3 and 4, cathode air pre-heating.

Examining alternative 1, it was found that system efficiency decreased compared to the base case. This is mainly due to an increased back pressure at the cathode feed line as a consequence of the additional pressure drop inside the afterburner. Furthermore, the first alternative design requires a somewhat larger heat exchanging area due to smaller temperature differences in the steam generator and air pre-heater. On the other hand, only two instead of three air blowers are needed, thus reducing costs and space requirements.

The net electric efficiency of alternative 2 increased compared to the base case. Thus, the positive effect of higher system fuel utilization dominates over the negative effects of lower stack voltage and increased system-intrinsic power consumption. Due to the increased fuel utilization, more excess air is needed to hold the stack at the specified operation temperature. On the other hand, less air has to be supplied to the afterburner since the anode off-gas contains a smaller amount of combustible compounds. As a consequence, condensate can be captured with less effort at higher temperature.

Cathode off-gas recirculation as realized in process alternative 3 leads to only a small increase in the total electric efficiency compared to the reference case, since the reduction in system-intrinsic power consumption is largely compensated by the reduced power output of the stack. The latter is a consequence of a decreased voltage due to oxygen depletion in the cathode feed, which is caused by recycling. The flow rate of fresh air to the cathode was reduced by a factor of four. This is a direct consequence of the high recirculation ratio (79%), which is required to maintain the specified operation temperature of the stack. Another consequence of cathode recycling is that the off-gas leaves the system with a significantly reduced flow rate but at elevated temperature.

Looking at system alternative 4, it was found that the effects of the single recycles, which were examined in alternatives 2 and 3, approximately add up. Compared to alternative 3 with cathode off-gas recycling, the lambda value, which is needed for isothermal operation of the SOFC, almost remains unchanged. Nevertheless, a larger absolute flow rate of air is needed since the fuel utilization increases due to the anode off-gas recycling. In relation to the base case, the net electric efficiency increases by almost 10%, while the required heat exchanging area is reduced by more than a factor of two. The latter is mainly due to the replacement of the cathode air pre-heater by anode off-gas recycling, which can neatly be illustrated in a temperature-enthalpy diagram using composite curves. Composite curves originate from pinch analysis with the aim of identifying the maximum possible heat recovery and the minimum energy requirement of a thermal or chemical process [47,48]. The hot composite curve represents all heat delivering streams condensed into a single curve. Likewise, the cold composite curve comprises all heat absorbing streams. Combined in the same diagram, they illustrate the overall heat transfer as it would occur if all heat was exchanged in a single heat exchanger. In the present cases, all external heat exchangers of the APU system and also the internal heat exchangers depicted in Figs. 1 and 2 are taken into account. Heat transfer associated with mixing of hot and cold streams, which theoretically could be considered by introducing virtual heat exchangers [49], is neglected. Fig. 6 shows that the composite curves of alternative 4 extend significantly less into the x-direction than those of the base case. As a consequence of

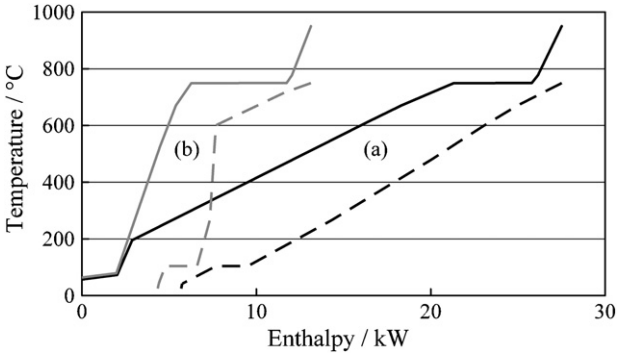

Fig. 6. Pinch diagram showing composite curves of base case (a) and system alternative 4 (b). Solid lines: hot composite curves (heat delivering streams); dashed lines: cold composite curves (heat absorbing streams).

Table 3
Power consumption (W) of blowers/compressors needed to convey the indicated gas streams.

	Base case	Alt. 1	Alt. 2	Alt. 3	Alt. 4
Air supply to ATR	40	50	40	40	40
Cathode air supply	418	481	519	24	29
Anode recycle	–	–	36	–	36
Cathode recycle	–	–	–	271	333
Combustion air (burner)	20	–	6	20	7
Cooling air (condenser)	54	50	42	54	42

this decreased heat exchange, the minimal required overall heat exchanging area can be reduced, which is in agreement with the last row of Table 2. Yet another conclusion can be drawn from Fig. 6: Since both composite curves are aligned to the right without generating pinch points or intersections, the thermal power required to heat up all cold streams can completely be delivered internally from the hot streams.

If system alternative 4 could be realized without any parasitic power losses, theoretically an AC efficiency of 35.4% could be obtained, which implies another potential increase of 10.6%. Thus, a first step towards further system optimization is the identification of the main contributors to system-intrinsic power consumption. These are the gas blowers and compressors, the AC power needs of which are summarized in Table 3. The cathode air blower is clearly identified as the main consumer in systems without cathode recycling. In contrast, if cathode recirculation loops are present, the blower inside the recycle loop contributes most to the overall consumption.

4.2. Sensitivity analysis

In the previous section, the system efficiency of an SOFC-APU was optimized by varying the process layout. Constant process parameters were assumed, with their respective values adjusted to the state of the art. However, future technological development will potentially yield improvements in most system components. In order to examine the resulting potential for a further enhancement of system efficiency, a sensitivity analysis was conducted. As indicated in Table 4, four critical process parameters were selected. Each of these parameters was varied between two stages: the actual value and an assumed improved value. Since the aim was to identify an optimized APU system, the sensitivity analysis was based on process alternative 4.

The schematic of the applied 2^4 factorial design is outlined in Table 5. It contains four main factors (F1, F2, F3 and F4) which correspond to the process parameters introduced in Table 4. The larger and smaller values of the two stage variations are indicated by "+1" and "−1", respectively. Furthermore, all two-factor interactions (F12, F13, etc.) can be assessed in a straightforward manner, which is one major advantage of using a factorial design.From each of the 16 simulation results, the following four response variables were extracted for evaluation:

- Y_1: net electric efficiency of the system;
- Y_2: lambda of the stack as defined in Eq. (10);

Table 4
Minimum and maximum values of varied parameters.

Parameter	Number (F_i)	Actual value (level 1)	Improved value (level 2)
Blower efficiency	1	0.60	0.75
Oxygen-to-carbon ratio in ATR	2	0.47	0.45
Reference voltage (mV)	3	700	750
Stack fuel utilization	4	0.75	0.85

Table 5
2^4 factorial design – normalized factor levels of main factors and binary interaction factors.

Run j	Factor									
	F1	F2	F12	F3	F13	F23	F4	F14	F24	F34
1	−1	−1	+1	−1	+1	+1	−1	+1	+1	+1
2	+1	−1	−1	−1	−1	+1	−1	−1	+1	+1
3	−1	+1	−1	−1	+1	−1	−1	+1	−1	+1
4	+1	+1	+1	−1	−1	−1	−1	−1	−1	+1
5	−1	−1	+1	+1	−1	−1	−1	+1	+1	−1
6	+1	−1	−1	+1	+1	−1	−1	−1	+1	−1
7	−1	+1	−1	+1	−1	+1	−1	+1	−1	−1
8	+1	+1	+1	+1	+1	+1	−1	−1	−1	−1
9	−1	−1	+1	−1	+1	+1	+1	−1	−1	−1
10	+1	−1	−1	−1	−1	+1	+1	+1	−1	−1
11	−1	+1	−1	−1	+1	−1	+1	−1	+1	−1
12	+1	+1	+1	−1	−1	−1	+1	+1	+1	−1
13	−1	−1	+1	+1	−1	−1	+1	−1	−1	+1
14	+1	−1	−1	+1	+1	−1	+1	+1	−1	+1
15	−1	+1	−1	+1	−1	+1	+1	−1	+1	+1
16	+1	+1	+1	+1	+1	+1	+1	+1	+1	+1

- Y_3: standard flow rate of air to the cathode;
- Y_4: lambda of the afterburner as defined in Eq. (18).

The factorial design (Table 5) constitutes a matrix with elements c_{ij} varying between −1 and +1. According to [50], this allows for the calculation of quantitative effects of all factors i on a response variable Y_k:

$$E_{k,i} = \frac{1}{0.5\ \mathrm{N}} \sum_{j=1}^{N} (c_{ij} Y_{k,j}) \tag{22}$$

The sum in Eq. (22), called a contrast, comprises all $N = 16$ calculated values $Y_{k,j}$. In order to allow for comparison of the effects on different response variables, relative effects are defined:

$$e_{k,i} = \frac{E_{k,i}}{(1/N)\sum_{j=1}^{N} Y_{k,j}} = \frac{E_{k,i}}{\bar{Y}_k} \tag{23}$$

In Fig. 7, the relative effects are plotted against the four main and six interaction factors.

First of all, Fig. 7 clearly shows that the effects of the interaction factors are small compared to those of the main factors. The effects of the main factors are discussed in detail.

- Blower efficiency (F1): Increasing the adiabatic efficiency of the blowers from 0.6 to 0.75 improves the net electric efficiency of the system by approximately 2%. The decrease in the power dissipation of the adiabatic blowers leads to lower blower out-

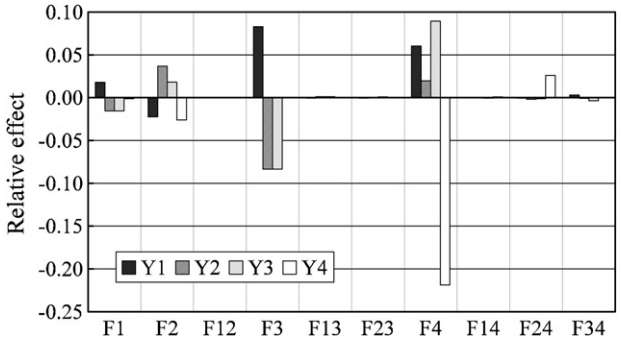

Fig. 7. Relative effects of the main factors (cf. Table 4) and interaction factors on net electric efficiency (Y1), air-to-fuel ratio of the stack (Y2), standard flow rate of air to the cathode (Y3) and air-to-fuel ratio of the burner (Y4).

let temperatures. As a consequence, the amount of excess air required to cool the stack decreases.
- Oxygen-to-carbon ratio in the ATR (F2): More liquid fuel is converted by endothermic steam reforming and less by exothermic partial oxidation when $n(O_2)/n(C)$ decreases from 0.47 to 0.45. As a result, more hydrogen is produced per mole of fuel and consequently the net electric efficiency of the whole system (Y_1) increases. Furthermore, reformate leaves the ATR at a temperature, which is lower by 25 °C, resulting in an increased methane content. A lower reformate temperature and increased rates of endothermic methane steam reforming in the SOFC mean that less excess air has to be supplied to the stack for cooling (cf. [51]). In this regard, the normalized air-to-fuel ratio (Y_2) appears to be more affected than the flow rate of air (Y_3). However, this merely refers to the fact that the absolute flow rate of utilizable fuel gas increases as a result of the higher rate of steam reforming. Finally, decreasing the oxygen-to-carbon ratio has an unfavorable effect on the amount of fresh air required for uncritical operation of the afterburner (Y_4). This is caused by the lower overall mass flow rate of anode off-gas, which simultaneously contains a larger amount of combustible compounds.
- Reference voltage (F3): Qualitatively, F3 causes the same effects as F1. However, the absolute values of the effects are almost five times larger, which can be ascribed to the large impact of the stack voltage on the response variables Y_1 to Y_3. These are more directly affected by F3 compared to F1.
- Stack fuel utilization (F4): Increasing stack utilization from 0.75 to 0.85 improves the net electric system efficiency by 6%. However, more air is needed to maintain the specified operation temperature of 750 °C. Interestingly, the relative effect on the absolute air flow is 4.5 times larger than the effect on lambda. This is due to the definition of lambda in Eq. (10), which accounts for the utilized fuel instead of the total fuel flow rate. Moreover, increasing the fuel utilization significantly lowers the concentration of combustible compounds in the anode off-gas. As a consequence, less fresh air is required to limit the adiabatic combustion temperature in the burner, resulting in a very large effect of factor F4 on the lambda of the afterburner (Y_4).

Only one significant interaction effect was observed: the effect of F24 on the normalized air-to-fuel ratio of the afterburner (Y_4). F24 describes the interaction between the ATR's oxygen-to-carbon ratio (F2) and stack fuel utilization (F4); it indicates that the effect of F2 on Y_4 is different at different factor levels of F4. In the present case, however, this simply originates from a process constraint: at high fuel utilization, i.e. at the upper level of factor F4, the response variable Y_4 cannot adjust freely to F2 but remains at the minimal allowable value of 1.1.

As stated at the beginning of this section, the main goal of the sensitivity analysis was to evaluate the potential for improving system performance by parameter variation. For the purpose of quantification, a first-order regression polynomial was derived on the basis of the relative effects. Within the limits of all $I = 10$ factors ($-1 \le c_i \le 1$), the response variables can be calculated as follows:

$$Y_k = \left(1 + \sum_{i=1}^{I} c_i \frac{e_{k,i}}{2}\right) \bar{Y}_k \tag{24}$$

The final, parameter-optimized system is based on the process layout of alternative 4 (Fig. 5) and is thus denoted alternative 4*. Compared to alternative 4, system fuel utilization increases to 91.9% and intrinsic electric power consumption decreases to only 0.38 kW. As a consequence, a net electric efficiency of 38.5% is reached for alternative 4*. It exhibits an SOFC lambda of 2.0, a corresponding air standard flow rate of 19 $m^3\,h^{-1}$ and a standard flow rate of air to the afterburner of only 0.9 $m^3\,h^{-1}$. Furthermore, the standard flow rate of effective off-gas is as low as 25.3 $m^3\,h^{-1}$ at 517 °C. Only 0.47 m^2 of heat exchanging area is needed. Thus, except for the condensation temperature, which increases to a value of 66 °C, all process targets could be improved by parameter optimization.

5. Conclusion

A thermodynamic model for numerical simulations of solid oxide fuel cell systems including autothermal reforming was presented. The approach is based completely on highly developed process simulation software, which allows building and varying complex system layouts with only limited effort.

A conceptual study was conducted, in which five different process designs of an SOFC-based auxiliary power unit were analyzed and compared to each other. Gains in system efficiency could be achieved, however at the cost of more complex system designs. Compared to the reference case, the high-efficiency system contains a cathode and an anode recycle loop. In order to evaluate further optimization potentials, a parametric study was conducted, including four critical process parameters associated with different system components. Using techniques from the design and analysis of experiments, factor effects were quantified and linear regression polynomials could be extracted. By combining the optimized process design and optimized process parameters, a net electric system efficiency of 38.5% was achieved, which corresponds to an increase of almost 10% points compared to the reference system. These theoretical findings may serve as guidelines for the future development of prototype or even close-to-production systems.

One of the main obstacles to a further improvement of the fuel cell system performance was found in intrinsic electric power consumption. The blowers, which deliver air to the cathode, were identified as the main consumers. Thus, since air is the primary cooling medium for the fuel cell stack, alternative stack-cooling concepts are desirable. Possible designs for such alternative cooling concepts will be examined in a forthcoming study.

Acknowledgement

The authors would like to thank R. Menzer for his valuable work, which built the basis for the present model.

References

[1] N. Lutsey, J. Wallace, C.-J. Brodrick, H.A. Dwyer, D. Sperling, Modeling Stationary Power for Heavy-duty Trucks: Engine Idling vs. Fuel Cell APUs, Technical Paper 2004-01-1479, SAE International, 2004.
[2] F. Baratto, U.M. Diwekar, D. Manca, J. Power Sources 139 (1–2) (2005) 205–213.
[3] P. Agnolucci, Int. J. Hydrogen Energy 32 (17) (2007) 4306–4318.
[4] M. Santarelli, M. Cabrera, M. Cali, J. Fuel Cell Sci. Technol. 7 (2) (2010).
[5] J. Lawrence, M. Boltze, J. Power Sources 154 (2) (2006) 479–488.
[6] A. Lindermeir, S. Kah, S. Kavurucu, M. Mühlner, Appl. Catal. B: Environ. 70 (1–4) (2007) 488–497.
[7] C. Mengel, M. Konrad, R. Wruck, K. Lucka, H. Köhne, J. Fuel Cell Sci. Technol. 5 (2) (2008).
[8] Q. Ming, P. Irving, J. Berry, A. Reis, Fuel Cells Bull. (1) (2010) 12–15.
[9] M. O'Connell, G. Kolb, K.-P. Schelhaas, J. Schürer, A. Ziogas, V. Hessel, Chem. Eng. Technol. 32 (11) (2009) 1790–1798.
[10] I. Kang, Y. Kang, S. Yoon, G. Bae, J. Bae, Int. J. Hydrogen Energy 33 (21) (2008) 6298–6307.
[11] I. Kang, S. Yoon, G. Bae, J. Kim, S. Baek, J. Bae, J. Fuel Cell Sci. Technol. 7 (3) (2010).
[12] S. Yoon, S. Lee, J. Bae, Development of a self-sustaining kWe-class integrated diesel fuel processing system for solid oxide fuel cells , Int. J. Hydrogen Energy (2010), doi:10.1016/j.ijhydene.2010.10.001.
[13] S. Roychoudhury, C. Junaedi, D. Walsh, et al., Proceedings of the 2008 Fuel Cell Seminar, Phoenix, AR, 2008.
[14] J. Pasel, J. Meißner, Z. Porš, R.C. Samsun, A. Tschauder, R. Peters, Int. J. Hydrogen Energy 32 (18) (2007) 4847–4858.
[15] Z. Porš, J. Pasel, A. Tschauder, R. Dahl, R. Peters, D. Stolten, Fuel Cells 8 (2) (2008) 129–137.
[16] P. Lamp, J. Tachtler, O. Finkenwirth, S. Mukerjee, S. Shaffer, Fuel Cells 3 (3) (2003) 146–152.
[17] http://delphi.com/manufacturers/cv/fuelcells (April 2011).

[18] L. Petruzzi, S. Cocchi, F. Fineschi, J. Power Sources 118 (1–2) (2003) 96–107.
[19] H.H. Dobbs, T. Krause, R. Kumar, M. Krumpelt, A.J. McEvoy, Proc. 4th European Solid Oxide Fuel Cell Forum, Luzern, Switzerland, 2000.
[20] M. Sorrentino, C. Pianese, J. Fuel Cell Sci. Technol. 6 (4.) (2009).
[21] S. Baek, Y. Kim, J. Bae, Proc. 6th International Conference on Fuel Cell Science, Engineering, and Technology, ASME, Denver, CO, 2008, pp. 645–651.
[22] C. Schlitzberger, R. Leithner, H. Zindler, J. Fuel Cell Sci. Technol. 6 (4) (2009).
[23] S. Farhad, F. Hamdullahpur, Y. Yoo, Int. J. Hydrogen Energy 35 (8) (2010) 3758–3768.
[24] R. Bove, P. Lunghi, N.M. Sammes, Int. J. Hydrogen Energy 30 (2) (2005) 181–187.
[25] J. Palsson, A. Selimovic, L. Sjunnesson, J. Power Sources 86 (1–2) (2000) 442–448.
[26] W. Zhang, E. Croiset, P.L. Douglas, M.W. Fowler, E. Entchev, Energy Convers. Manage. 46 (2) (2005) 181–196.
[27] S. Campanari, J. Power Sources 92 (1–2) (2001) 26–34.
[28] K.D. Panopoulos, L.E. Fryda, J. Karl, S. Poulou, E. Kakaras, J. Power Sources 159 (1) (2006) 570–585.
[29] W. Doherty, A. Reynolds, D. Kennedy, J. Electrochem. Soc. 157 (7) (2010) B975–B981.
[30] E. Riensche, J. Meusinger, U. Stimming, G. Unverzagt, J. Power Sources 73 (2) (1998) 251–256.
[31] Simsci-Esscor, PRO/II 8.3 User Guide , Invensys Systems, Inc., Lake Forest, CA, September 2009.
[32] E. Achenbach, J. Power Sources 49 (1–3) (1994) 333–348.
[33] L. Andreassi, C. Toro, S. Ubertini, J. Fuel Cell Sci. Technol. 6 (2.) (2009).
[34] E. Achenbach, E. Riensche, J. Power Sources 52 (2) (1994) 283–288.
[35] H. Timmermann, W. Sawady, R. Reimert, E. Ivers-Tiffee, J. Power Sources 195 (1) (2010) 214–222.
[36] M. Pfafferodt, P. Heidebrecht, M. Stelter, K. Sundmacher, J. Power Sources 149 (2005) 53–62.
[37] C.O. Colpan, I. Dincer, F. Hamdullahpur, Int. J. Hydrogen Energy 32 (7) (2007) 787–795.
[38] A.L. da Silva, C.F. Malfatti, I.L. Müller, Int. J. Hydrogen Energy 34 (2009) 4321–4330.
[39] E.D. Sloan, in: N.P. Chopey (Ed.), Handbook of Chemical Engineering Calculations, McGraw-Hill, New York, 2004, pp. 12–13 (Chapter 4).
[40] I. Bahrin, G. Platzki, Thermochemical Data of Pure Substances, vol. 1–2, 3rd edition, VCH, Weinheim, 1995.
[41] J.G. Xu, G.F. Froment, AIChE J. 35 (1) (1989) 88–96.
[42] P.K. Cheekatamarla, A.M. Lane, J. Power Sources 152 (1) (2005) 256–263.
[43] J. Stalling, Evaluation of Microstructures for Application in Mobile Fuel Processing Units, PhD thesis, RWTH Aachen, 2003.
[44] H.C. Van Ness, M.M. Abbott, in: D.W. Green, J.O. Maloney (Eds.), Perry's Chemical Engineer's Handbook, 7th edition, McGraw-Hill, New York, 1997, pp. 24–30 (Chapter 4).
[45] J.D.J. Bankston, F.E. Baker, Selecting the Proper Pump , Southern Regional Aquaculture Center, 1994, SARC Publication No. 372.
[46] X. Zhang, J. Li, G. Li, Z. Feng, J. Power Sources 164 (2) (2007) 752–760.
[47] B. Linnhoff, W. Lenz, Chem. Ing. Tech. 59 (11) (1987) 851–857.
[48] J. Godat, F. Marechal, J. Power Sources 118 (1–2) (2003) 411–423.
[49] J. De Ruyck, V. Lavric, D. Baetens, V. Plesu, Energy Convers. Manage. 44 (14) (2003) 2321–2329.
[50] D.C. Montgomery, G.C. Runger, N.F. Hubele, Engineering Statistics , 4th edition, John Wiley & Sons, Inc., New York, 2007.
[51] R. Peters, R. Dahl, U. Klüttgen, C. Palm, D. Stolten, J. Power Sources 106 (1–2) (2002) 238–244.